Constraints on collective density variables: Two dimensions

Obioma U. Uche,[1] Frank H. Stillinger,[2] and Salvatore Torquato[2,3,*]
[1]*Department of Chemical Engineering, Princeton University, Princeton, New Jersey 08544, USA*
[2]*Department of Chemistry, Princeton University, Princeton, New Jersey 08544, USA*
[3]*Princeton Materials Institute, Princeton University, Princeton, New Jersey 08544, USA*
(Received 15 February 2004; published 28 October 2004)

Collective density variables $\rho(\boldsymbol{k})$ have proved to be useful tools in the study of many-body problems in a variety of fields that are concerned with structural and kinematic phenomena. In spite of their broad applicability, mathematical understanding of collective density variables remains an underexplored subject. In this paper, we examine features associated with collective density variables in two dimensions using numerical exploration techniques to generate particle patterns in the classical ground state. Particle pair interactions are governed by a continuous, bounded potential. Our approach involves constraining related collective parameters $C(\boldsymbol{k})$, with wave vector $\boldsymbol{k}$ magnitudes at or below a chosen cutoff, to their absolute minimum values. Density fluctuations for those $\boldsymbol{k}$'s thus are suppressed. The resulting investigation distinguishes three structural regimes as the number of constrained wave vectors is increased—disordered, wavy crystalline, and crystalline regimes—each with characteristic distinguishing features. It should be noted that our choice of pair potential can lead to pair correlation functions that exhibit an effective hard core and thus signal the formation of a hard-disk-like equilibrium fluid. In addition, our method creates particle patterns that are hyperuniform, thus supporting the notion that structural glasses can be hyperuniform as the temperature $T \to 0$.

DOI: 10.1103/PhysRevE.70.046122 PACS number(s): 05.70.Fh, 05.20.Jj

I. INTRODUCTION

Understanding, predicting, and manipulating the spatial patterns of particles in many-body systems remain continuing challenges to condensed matter science. Collective density variables offer a useful analytical tool in this context. If N identical point particles reside in a region Ω at positions $\boldsymbol{r}_1, \ldots, \boldsymbol{r}_N$, subject to periodic boundary conditions, the collective density variables $\rho(\boldsymbol{k})$ are defined thus:

$$\rho(\boldsymbol{k}) = \sum_{j=1}^{N} \exp(i\boldsymbol{k} \cdot \boldsymbol{r}_j). \tag{1.1}$$

Here the wave vectors denoted by $\boldsymbol{k}$ are those appropriate for region Ω. Specific applications in which these quantities have played important descriptive roles are the random-phase approximation for conduction electrons in metals [1], phonons in superfluid ^{4}He [2], crystal nucleation and growth in simulated supercooled liquids [3], and the development of integral equations for description of short-range order in fluids [4,5]. An additional physical application involves mode-coupling theory as applied to the study of relaxation dynamics of density fluctuations in supercooled liquids [6,7].

Configurations that are subject to minimized collective density variables have potential applications in a number of diverse fields. In the material science context, it may be desirable to fabricate amorphous materials that suppress radiation scattering over a range of long wavelengths without producing strong Bragg reflections. An additional application involves the determination of animal territory size and shape in the ecological domain [8]. In particular, the configurations could be used as ideal arrangements for comparison to ecological field cases. Alternatively, the configurations might serve as initial conditions for investigations in the dynamics of gravity collapse [9].

The nonlinearity of the transformation (1.1) from the finite set of particle coordinates $\boldsymbol{r}_1, \ldots, \boldsymbol{r}_N$ to the infinite set of $\rho(\boldsymbol{k})$ generates a variety of nontrivial features. These were explored to some extent for one-dimensional systems in a previous paper [10], which was specifically concerned with the effects of forcing sets of density fluctuations to vanish. The objective of the present contribution is to extend that former study to two-dimensional systems. Our primary tool for doing so is numerical simulation of a variety of finite particle systems. As explained below, the results emerging from this investigation have implications for phase transition theory, and for the theory of "hyperuniform" systems [11].

The following section contains the basic formulas required for this analysis. Section III provides details of the numerical procedures that we have employed in this study. Sections IV and V present our results on particle patterns and Voronoi tessellations. Conclusions and related discussion appear in the final section.

II. BASIC FORMULAS

A natural choice for the two-dimensional region Ω is a rectangle with side lengths L_x and L_y. The corresponding infinite set of wave vectors is

$$\boldsymbol{k} = (2\pi n_x/L_x, 2\pi n_y/L_y), \tag{2.1}$$

where the n_x and n_y are positive or negative integers, or zero. With the exception of $\rho(0) \equiv N$, the $\rho(\boldsymbol{k})$ are complex and

*Corresponding author.
Electronic address: torquato@princeton.edu

vary with the N-particle configuration, but are bounded above and below in magnitude:

$$0 \leqslant |\rho(\boldsymbol{k})| \leqslant N \quad (\boldsymbol{k} \neq 0). \tag{2.2}$$

For present purposes, it is more convenient to work with the real quantities $C(\boldsymbol{k})$ defined by [10]

$$\rho(\boldsymbol{k})\rho(-\boldsymbol{k}) = |\rho(\boldsymbol{k})|^2 = N + 2C(\boldsymbol{k}), \tag{2.3}$$

$$C(\boldsymbol{k}) = \sum_{j=1}^{N-1} \sum_{l=j+1}^{N} \cos[\boldsymbol{k} \cdot (\boldsymbol{r}_j - \boldsymbol{r}_l)]. \tag{2.4}$$

These are subject to the following constraints:

$$C(0) = \frac{1}{2}N(N-1),$$

$$C(\boldsymbol{k}) = C(-\boldsymbol{k}),$$

$$-\frac{1}{2}N \leqslant C(\boldsymbol{k}) \leqslant \frac{1}{2}N(N-1) \quad (\boldsymbol{k} \neq 0). \tag{2.5}$$

The corresponding structure factor $S(\boldsymbol{k})$ for a single configuration can be expressed in terms of the $C(\boldsymbol{k})$ quantities

$$S(\boldsymbol{k}) = 1 + \frac{2}{N}\sum_{j=1}^{N-1} \sum_{l=j+1}^{N} \cos[\boldsymbol{k} \cdot (\boldsymbol{r}_j - \boldsymbol{r}_l)] = 1 + \frac{2}{N}C(k). \tag{2.6}$$

Suppose that the particles interact pairwise with an isotropic pair potential $v(\boldsymbol{r}_{jl})$, so that the total energy function is

$$\Phi(\boldsymbol{r}_1, \ldots, \boldsymbol{r}_N) = \sum_{j<l} v(\boldsymbol{r}_{jl}). \tag{2.7}$$

Suppose furthermore that this pair potential has a Fourier transform $V(\boldsymbol{k})$:

$$V(\boldsymbol{k}) = \int_{\Omega} v(\boldsymbol{r}) \exp(i\boldsymbol{k} \cdot \boldsymbol{r}) d\boldsymbol{r},$$

$$v(\boldsymbol{r}) = \Omega^{-1} \sum_{\boldsymbol{k}} V(\boldsymbol{k}) \exp(-i\boldsymbol{k} \cdot \boldsymbol{r}), \tag{2.8}$$

where in the last expression the summation covers the entire set of $\boldsymbol{k}$'s. Then it is straightforward to show that the total potential energy for the N-particle system can be exactly expressed in the following manner in terms of the real collective density variables [10]:

$$\Phi = \Omega^{-1} \sum_{\boldsymbol{k}} V(\boldsymbol{k}) C(\boldsymbol{k}). \tag{2.9}$$

By virtue of the fact that both $C(\boldsymbol{k})$ and $V(\boldsymbol{k})$ are inversion invariant, the last sum could be restricted to the origin, plus one half of the $\boldsymbol{k} \neq 0$ space with a compensating factor of 2.

For the purposes of the present investigation, we will place special emphasis on pair interactions whose transform $V(\boldsymbol{k})$ possesses the following characteristics:

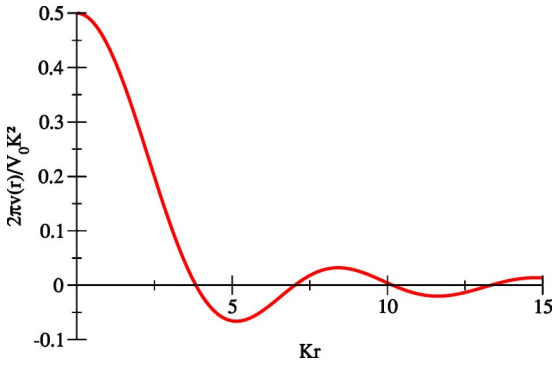

FIG. 1. A scaled plot of the pair interaction defined by Eq. (2.11).

$$V(\boldsymbol{k}) = \begin{cases} V_0 > 0 & (0 \leqslant |\boldsymbol{k}| \leqslant K), \\ 0 & (K < |\boldsymbol{k}|). \end{cases} \tag{2.10}$$

We choose this form for simplicity recognizing at the same time that any other positive $V(\boldsymbol{k})$ for $|\boldsymbol{k}| \leqslant K$ but zero otherwise would lead to the same results. In the large-Ω limit, with K held fixed, the simple Fourier transform (2.10) may be inverted to yield the following form for the pair interaction in real space:

$$v(r) = (V_0 K/2\pi r) J_1(Kr),$$

$$v(r) \sim \left(\frac{V_0 K^{1/2}}{2^{1/2}\pi^{3/2} r^{3/2}}\right) \cos(Kr - 3\pi/4) \quad (r \to +\infty), \tag{2.11}$$

where as usual J_1 denotes the Bessel function of first order [12] and r is the distance. Figure 1 displays the particle-pair interaction in real space. It should be noted that this interaction potential is qualitatively similar to the weakly decaying Friedel oscillations observed in the screened potential of ions in molten metals [13].

If the $\boldsymbol{k}$-space range parameter K is small, the number of independent collective coordinates $C(\boldsymbol{k})$ in Eq. (2.9) included within this radius will only be a small fraction of the number of degrees of freedom $2N$ present in the system. Using earlier one-dimensional results as a guide [10] it is then expected that the classical ground state of the system, the absolute minimum of Φ, will be attained for that set of configurations with all of those included $C(\boldsymbol{k})$'s driven to their minimum values $-N/2$. As radius K increases to cover larger and larger numbers of the $C(\boldsymbol{k})$'s, and consequently having an impact on a larger and larger fraction of the total degrees of freedom, the result for the classical ground state is far from obvious. Clarifying this situation forms the objective of Secs. III–V.

III. NUMERICAL SEARCH PROCEDURE

We have devoted our numerical activity to examination of ground-state configurations for the N-particle system, subject to the type of pair interaction specified by Eq. (2.10). Interest centers about the effects of varying the $\boldsymbol{k}$-space cutoff radius K. A single simplifying assumption has been invoked. In all subsequent calculations, we assume that the system area Ω is

TABLE I. Successive rational approximations p/q to the irrational number $3^{1/2}$. The implied system sizes to permit a nearly undeformed triangular lattice to fit within a square region Ω are the product of integers $N=2pq$; the corresponding configuration consists of $2q$ rows of p particles.

p	q	p/q	$\lvert 3^{1/2}-p/q\rvert$	N
1	1	1.000000	0.732051	2
2	1	2.000000	0.267949	4
3	2	1.500000	0.232051	12
5	3	1.666667	0.065384	30
7	4	1.750000	0.017949	56
12	7	1.714286	0.017765	168
19	11	1.727273	0.004778	418
26	15	1.733333	0.0012825	780
45	26	1.730769	0.0012816	2340
71	41	1.731707	0.00034349	5822
97	56	1.732143	0.000092049	10864

a unit square ($L_x=L_y=L=1$), to which periodic boundary conditions apply.

The majority of our calculations have chosen the number of particles N to be such that they could be assembled in the square container in a nearly undeformed version of the triangular crystal. Results to be presented in the following Sec. IV justify this tactical choice. In particular, such an ideal configuration would consist of $2q$ rows of particles, each aligned with container sides and containing p equally spaced particles, where the rational number p/q is a close approximation to the irrational number $3^{1/2}$. Table I shows a set of possible p,q choices, indicating how good an approximation to the ideal irrational ratio each choice represents.

For any given choice of N and K, the majority of our numerical studies utilized a random number generator to create an initial configuration of the particles inside the square container Ω. This starting point typically produces a large positive value of the system potential energy Φ. The next step involved use of the conjugate gradient method [14] to seek a particle configuration that yielded the absolute minimum value of Φ. The conjugate gradient method locates a local minimum of the given function provided that its gradient can be computed, which is the case for the present application.

If the number of $\boldsymbol{k}$ vectors at or inside cutoff K is denoted by $2M(K)+1$, and if all of the corresponding $C(\boldsymbol{k})$ could be driven to their minimum values in this configuration search, then that absolute Φ minimum would be equal to $(NV_0/2)\times[1-2M(K)]$. Then because $S(\boldsymbol{k})=0$ for those $\boldsymbol{k}$'s at which $C(\boldsymbol{k})$ has been minimized, the resulting configurations are hyperuniform [11]. [Note that $M(K)$ is the number of independent collective coordinates within radius K.] For some of the larger N and K choices, the conjugate gradient procedure would converge to higher relative minima, requiring rejection and motivating a restart at a different random initial configuration. Table II contains a tabulation of the first few shells of $\boldsymbol{k}$ vectors surrounding the origin, and the corresponding M values.

TABLE II. Coordination number Z_i and squares of reduced distances $|\boldsymbol{k}_i|/|\boldsymbol{k}_1|$ for the square lattice of $\boldsymbol{k}$ vectors.

Shell	Z_i	$(\lvert\boldsymbol{k}_i\rvert/\lvert\boldsymbol{k}_1\rvert)^2$	$M(\lvert\boldsymbol{k}_i\rvert/\lvert\boldsymbol{k}_1\rvert)$
1	4	1	2
2	4	2	4
3	4	4	6
4	8	5	10
5	4	8	12
6	4	9	14
7	8	10	18
8	8	13	22
9	4	16	24
10	8	17	28
11	4	18	30
12	8	20	34
13	12	25	40
14	8	26	44
15	8	29	48
16	4	32	50
17	8	34	54
18	4	36	56
19	8	37	60
20	8	40	64
⋮	⋮	⋮	⋮
50	8	117	186
⋮	⋮	⋮	⋮
115	8	306	486
⋮	⋮	⋮	⋮
150	16	410	652

IV. RESULTS—PARTICLE PATTERNS

Our numerical studies included several system sizes, various M values, and collections of initial configurations (both random and lattice-based). Calculations were carried out to high precision with the system potential energy Φ converging to its absolute minimum. It should be noted that at high M values, some random initial configurations in fact did not converge to the absolute minimum, as indicated above. Evidently, the Φ hypersurface for those cases contained a substantial population of relative minima that lay above the classical ground state. However, the conjugate gradient trajectories converged to the absolute Φ minimum in all cases included in our final analysis. Table III displays a summary of the investigated systems. Our findings showed a qualitatively consistent pattern for all system sizes.

In order to simplify our analysis, we introduce the parameter

$$\chi=\frac{M(K)}{2N}, \tag{4.1}$$

which is the ratio of the constrained degrees of freedom to the total number of degrees of freedom. We have observed

TABLE III. Conjugate gradient numerical studies were performed on the following systems for the indicated range of $M(K)$ values. All systems included in our final analysis converged to the absolute Φ minimum.

N	Range of $M(K)$ values
12	$0 \leqslant M(K) \leqslant 18$
56	$0 \leqslant M(K) \leqslant 84$
168	$0 \leqslant M(K) \leqslant 244$
418	$0 \leqslant M(K) \leqslant 652$

three distinct regimes of the final configurations as χ varies: disordered, wavy crystalline, and crystalline. Table IV presents the ranges in χ for differing system sizes and regimes. This table shows that the disordered regime for particle configurations corresponds to low values of χ. Likewise, high values of χ yield crystalline particle patterns. Numerical entries in Table IV strongly suggest that as N increases, the crossover χ value separating the disordered and wavy crystalline regimes approaches a limit around 0.58. By contrast, the corresponding crossover χ between the wavy crystalline and crystalline regimes exhibits a slow upward drift with N, and we are currently unable to decide if its large-N limit is less than, or equal to, unity. In the upcoming paragraphs, we will discuss features that are characteristic of configurations in these regimes.

A particle pattern within the disordered regime for $N=418$ is displayed in Fig. 2. The random point clustering and lack of any visible overall regularity is quite apparent. Another distinct property of the disordered regime involves the isolation of a locus of minimum $C(\boldsymbol{k})$'s in the corresponding $\boldsymbol{k}$-space plot as shown in Fig. 3. Here, only those $C(\boldsymbol{k})$'s within the range of the square mound $V(\boldsymbol{k})$ (inside the cutoff radius K) are forced to the minimum $-N/2$. All others (indicated as "wild" values in the legend) seem to be free to vary between the limits shown in Eq. (2.5).

As $C(\boldsymbol{k})$'s for a larger and larger set of wave vectors are constrained to their minimum values (increasing χ), some novel configuration features emerge. There is a progressive change from the disordered configurations to particle patterns that consist of particle columns that display a meandering displacement away from linearity. An example of such a pattern is displayed in Fig. 4 and is defined as a "wavy crystal." A strong indication that the particle configuration falls within the wavy crystalline regime is the induced minimization of additional $C(\boldsymbol{k})$'s outside radius K that are not directly constrained by the numerical search procedure. In particular,

TABLE IV. Classification of investigated cases associated with each of the three regimes.

N	Disordered	Wavy crystalline	Crystalline
12	$\chi < 0.500000$	$\chi = 0.50000$	$\chi \geqslant 0.583333$
56	$\chi < 0.571428$	$0.571428 \leqslant \chi < 0.660714$	$\chi \geqslant 0.660714$
168	$\chi < 0.571428$	$0.571428 \leqslant \chi < 0.714286$	$\chi \geqslant 0.714266$
418	$\chi < 0.576550$	$0.576550 \leqslant \chi < 0.779904$	$\chi \geqslant 0.779904$

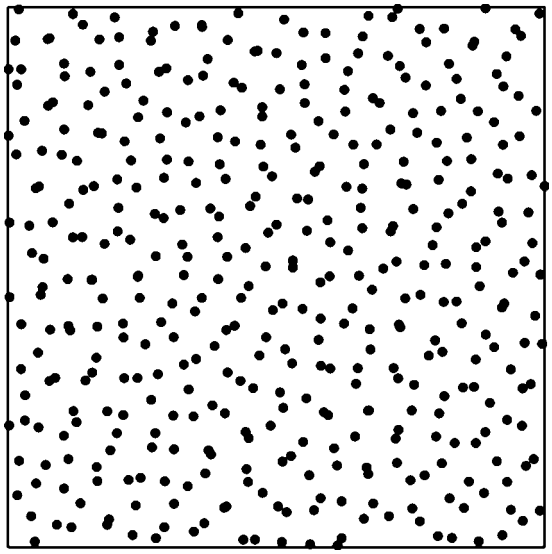

FIG. 2. Real space particle pattern in the disordered regime for a system of 418 point particles. The $C(\boldsymbol{k})$ quantities for the wave vectors confined within the 50th shell ($\chi=0.222488$) have been constrained to their minimum values $-N/2$.

Fig. 5 presents the $\boldsymbol{k}$-space plot for the particle pattern shown in Fig. 4. Two distinct characteristics of the wavy crystalline $\boldsymbol{k}$-space plot arise when Fig. 3 is compared to Fig. 5. The first of these traits is indicated by the presence of bands/patches of minimized $C(\boldsymbol{k})$'s beyond the locus of forcibly minimized $C(\boldsymbol{k})$ quantities. The other property involves the appearance of *peak* values for isolated $C(\boldsymbol{k})$'s. $C(\boldsymbol{k})$'s are labeled as peak values when they are within 50 percent of the maximum attainable $C(\boldsymbol{k})$ defined in Eq. (2.5). As in the disordered regime, most $C(\boldsymbol{k})$'s are free to fluctuate between the imposed limits.

For high values of the cutoff radius K, we observe a fully crystallized particle pattern devoid of waviness (see Fig. 6). It should be noted that for high values of χ, only a triangular

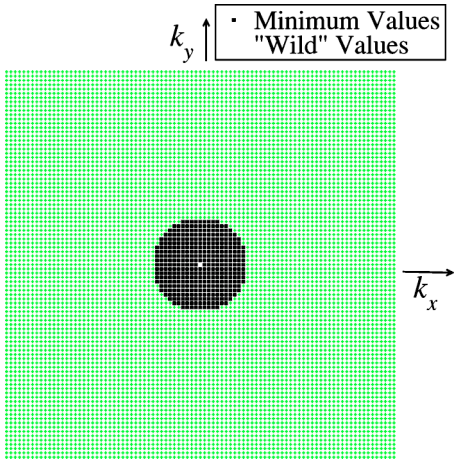

FIG. 3. $\boldsymbol{k}$-space plot of $C(\boldsymbol{k})$ values for a system of 418 point particles in the disordered regime. k_x ranges from -90π to 90π, as does k_y. The $C(\boldsymbol{k})$ quantities for the wave vectors confined within the 50th shell ($\chi=0.222488$) have been constrained to their minimum values $-N/2$ (see legend).

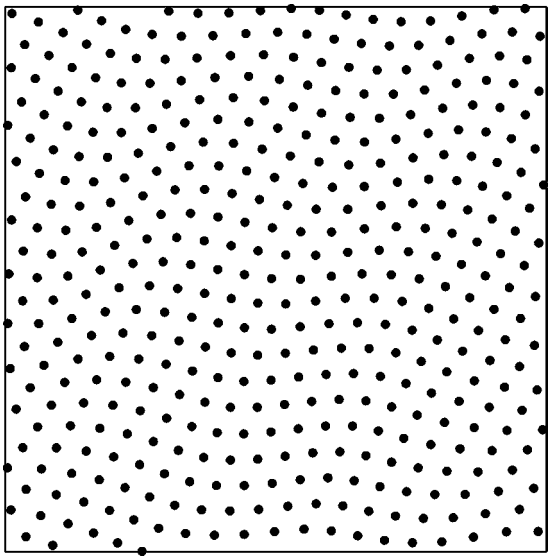

FIG. 4. Real space particle pattern in the wavy crystalline regime for a system of 418 point particles. The $C(\boldsymbol{k})$ quantities for the wave vectors confined within the 115th shell ($\chi=0.581340$) have been constrained to their minimum values $-N/2$.

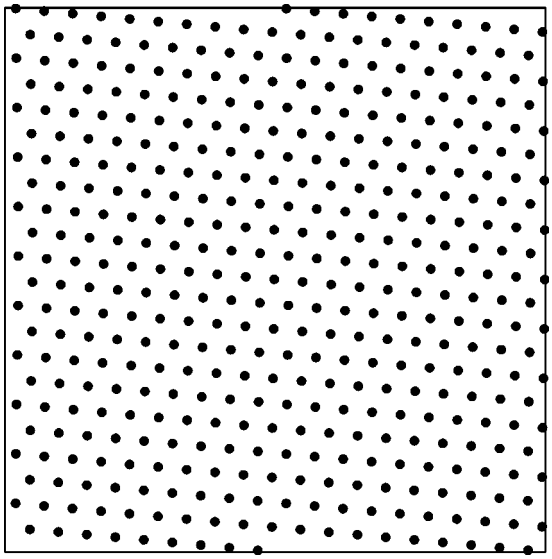

FIG. 6. Real space particle pattern in the crystalline regime for a system of 418 point particles. The $C(\boldsymbol{k})$ quantities for the wave vectors confined within the 150th shell ($\chi=0.779904$) have been constrained to their minimum values $-N/2$.

crystalline arrangement permits Φ to attain its absolute minimum. The corresponding $\boldsymbol{k}$-space plots (see Fig. 7) reveal that the $C(\boldsymbol{k})$ quantities are either minimized $(-N/2)$ or at their peak values $[\sim N(N-1)/2]$. However, for uniformly strained crystalline arrangements, some wildly fluctuating $C(\boldsymbol{k})$'s will occur in the vicinity of those exhibiting peak values. For both unstrained and strained crystals, the implicitly minimized $C(\boldsymbol{k})$'s exhibit a pattern that percolates throughout $\boldsymbol{k}$ space, as Fig. 7 illustrates.

In addition to the ideal N values listed in Table I, we investigated the effect of adding a single particle to the system size of interest and constraining a sufficient set of wave vectors such that χ was expected to fall within the crystalline regime. For such cases, we observe a rotated and strained crystalline particle pattern that fits all $N+1$ particles in the unit cell without any localized structural defect such as an interstitial particle.

Our numerical studies were extended to the use of lattice-based initial configurations. In particular, we utilized locally and globally perturbed rectangular arrays as inputs to our conjugate gradient algorithm. Point particles located on the sites of the rectangular lattice were perturbed by randomly displacing within the range $\delta_x=\pm 0.1 l_x$, $\delta_y=\pm 0.1 l_y$ for small perturbation and $\delta_x=\pm 0.5 l_x$, $\delta_y=\pm 0.5 l_y$ for large perturbation. Here, l_x and l_y are the distance between neighboring points in the lattice in the x and y directions. In general, we

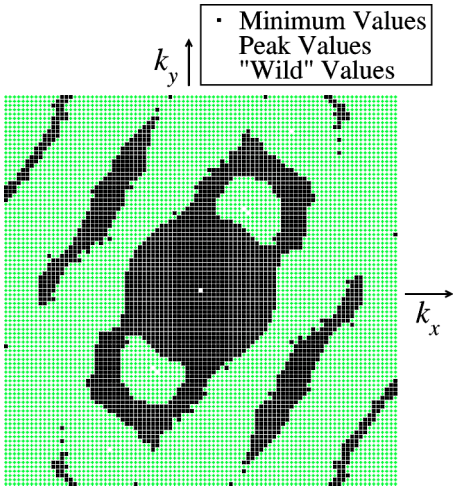

FIG. 5. $\boldsymbol{k}$-space plot of $C(\boldsymbol{k})$ values for a system of 418 point particles in the wavy crystalline regime. k_x ranges from -90π to 90π, as does k_y. The $C(\boldsymbol{k})$'s for the wave vectors confined within the 115th shell ($\chi=0.581340$) have been constrained to their minimum values $-N/2$ (see legend).

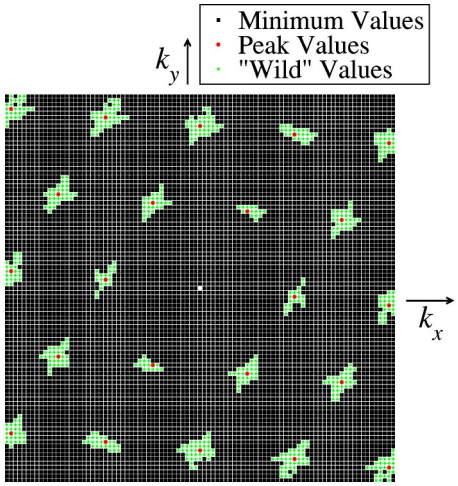

FIG. 7. $\boldsymbol{k}$-space plot of $C(\boldsymbol{k})$ values for a system of 418 point particles in the crystalline regime. k_x ranges from -90π to 90π, as does k_y. The $C(\boldsymbol{k})$'s for the wave vectors confined within the 150th shell ($\chi=0.779904$) have been constrained to their minimum values $-N/2$ (see legend).

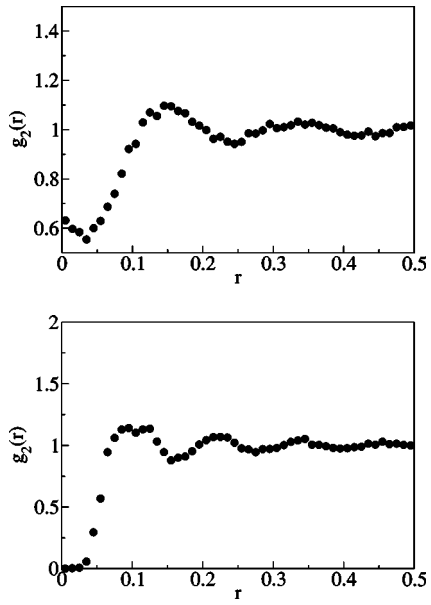

FIG. 8. Radial distribution function for systems of 168 point particles. Upper panel: The $C(\boldsymbol{k})$'s for the wave vectors confined within the 15th shell ($\chi=0.142857$) have been constrained to their minimum values $-N/2$. Fifty configurations have been sampled to create the RDF. Lower panel: The $C(\boldsymbol{k})$'s for the wave vectors confined within the 33rd shell ($\chi=0.345238$) have been constrained to their minimum values $-N/2$. Twenty-five configurations have been sampled to create the RDF.

were able to obtain the expected particle patterns and $\boldsymbol{k}$-space plots in the disordered and wavy crystalline regimes. However, the absolute Φ minimum was never attained for numerical searches at values of χ sufficiently high to be in the crystalline regime using either initial configuration.

Further insight into the generated point patterns can be obtained by study of their pair correlation functions. In particular, the possible emergence of an effective hard core diameter and the formation of a hard-disk-like equilibrium fluid, in spite of the fact that the pair interaction function is bounded and continuous, can be probed by inspection of the radial distribution function (RDF). The presence of clustered points at very low χ indicates that the effective hard core is likely to emerge only at higher values of χ. Figure 8 displays RDF's for configurations of point particles prior to ($\chi=0.142857$) and after ($\chi=0.345238$) the emergence of an effective hard core.

V. RESULTS—VORONOI TESSELLATIONS

In two dimensions, a Voronoi tessellation is a partitioning of space into convex polygonal cells [15,16]. It is alternatively known across various scientific disciplines as a Dirichlet tessellation or as Wigner-Seitz cells. In archeology, Voronoi polygons are used to map the spread of the use of tools in ancient cultures and for studying the influence of rival centers of commerce [17]. In ecology, the survival of an organism depends on the number of neighbors with which it must compete for food and light, and the Voronoi diagram of forest species and territorial animals is used to investigate the effect of overcrowding [18].

For any of the patterns discussed earlier, the set of N points with position coordinates $\boldsymbol{r}_1,\ldots,\boldsymbol{r}_N$ can be used as starting points for the generation of a Voronoi tessellation. The Voronoi cell is the polygonal space containing all positions closer to $\boldsymbol{r}_i$ than to any of the remaining $N-1$ points. The edges of the Voronoi cell are formed by segments of perpendicular bisectors to the lines connecting the point $\boldsymbol{r}_i$ to its nearest neighbor sites, i.e., to points $\boldsymbol{r}_j$ that share a Voronoi edge. The set of N Voronoi cells that are associated with the N points yields the Voronoi diagram. Finally, the full Voronoi tessellation can be generated by extending the Voronoi diagram to all space, making use of periodic boundary conditions.

Figures 9 and 10 show Voronoi tessellations for four point patterns. Voronoi polygon statistics for specific investigated systems (including those in Figs. 9 and 10) are displayed in Table V. The shape irregularity of the Voronoi polygons in both panels of Fig. 9 is visually clear. This common feature is not unexpected as relatively few constraints have been placed on the system in the lower panel of Fig. 9. However, the marked presence of size and shape homogeneity is apparent in the lower panel and not in the upper panel. By comparing the two panels in Fig. 10, one visually perceives both similarities and distinctions. The similarities concern the local regularity of the point patterns while the differences involve waviness in the upper point pattern in contrast to perfect periodicity on the lower.

The mean number of edges $\langle E\rangle$ and mean area $\langle A\rangle$ per Voronoi cell are constant for systems of the same size (square cell with $L=1$ and fixed N). The average number of edges per cell ($\langle E\rangle=6$) in two-dimensional Voronoi tessellations is an immediate consequence of Euler's theorem provided that all vertices have coordination number $Z=3$ [16]. A couple of observations can be made upon inspection of Table V. First, the downward trend in the standard deviation for both the number of edges and the area, for increasing values of χ, is apparent. Indeed, this trend is reflected in the higher degree of order in high χ systems.

In addition, we can explore comparisons between systems generated via our numerical search algorithm and the random sequential addition (RSA) process by contrasting of RDF's and Voronoi polygon statistics. A RSA configuration is produced by randomly, irreversibly, and sequentially placing nonoverlapping objects into a region [16]. The filling process terminates at the saturation limit of packing fraction $\phi\cong 0.55$ for identical hard disks in two dimensions. In performing the above comparison, we observe that the Voronoi tessellations of point particle systems of $\chi\cong 0.382775$ are qualitatively similar to RSA configurations at the saturation limit (see Fig. 8.4 of Ref. [14]). However, on closer numerical inspection there are clear differences that are not immediately apparent as measured by the abovementioned statistical attributes (see Table VI). It should be noted that despite varying χ values for the different statistical measures, all relevant particle configurations fall within the disordered regime. Furthermore, unlike our generated configurations, it is not known whether RSA configurations at the saturation density are hyperuniform.

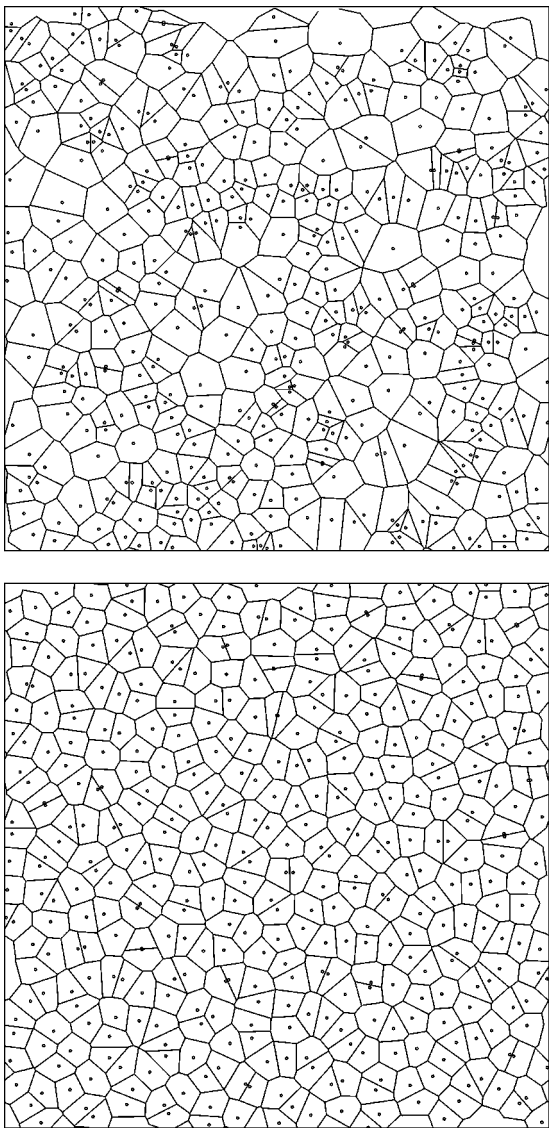

FIG. 9. Voronoi tessellations for configurations of point particles. Upper panel: Voronoi tessellation for an ideal gas distribution of 418 point particles. Lower panel: Voronoi tessellation for a system of 418 point particles for which all $C(\boldsymbol{k})$'s within the 50th shell ($\chi=0.222488$) have been constrained to their absolute minimum. The configuration falls within the disordered regime.

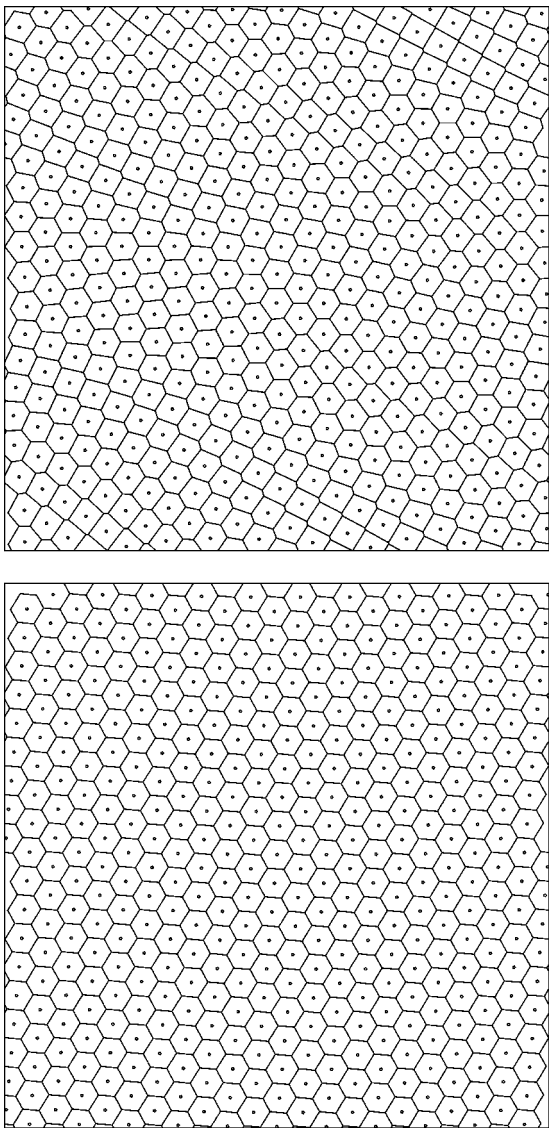

FIG. 10. Voronoi tessellation for configurations of point particles. Upper panel: Voronoi tessellation of a system of 418 point particles for which all $C(\boldsymbol{k})$'s within the 115th shell ($\chi=0.581340$) have been constrained to their absolute minimum. The configuration falls within the wavy crystalline regime. Lower panel: Voronoi tessellation for a system of 418 point particles for which all $C(\boldsymbol{k})$'s within the 150th shell ($\chi=0.779904$) have been constrained to their absolute minimum. The configuration falls within the crystalline regime.

VI. CONCLUSIONS AND DISCUSSION

The overall objective pursued in this paper involves construction and analysis of many-particle configurations in two dimensions, subject to sets of constraints on the collective coordinate values for those configurations. In particular, collective coordinates $C(\boldsymbol{k})$ for wave vectors subject to $0<|\boldsymbol{k}|\leqslant K$ have been forced to their absolute minimum values, where K is a variable cutoff. The resulting many-particle configurations (see Figs. 2, 4, and 6) which are governed by a continuous and bounded potential (2.11) belong to the class of "hyperuniform" systems. In particular, this supports the notion that structural glasses can in fact be hyperuniform as $T\rightarrow 0$. Hyperuniform systems are defined by vanishing of density fluctuations, i.e., of $S(\boldsymbol{k})$, in the large-wavelength limit [11]. This confirms a possibility advanced by Torquato and Stillinger [11]. But note also that the class of configurations generated by our conjugate gradient algorithm goes beyond the established concept of "hyperuniformity" in that it suppresses all density fluctuations with wavelengths greater than a finite cutoff specified by the parameter K.

Three qualitatively distinct regimes of particle patterns have emerged from our calculations. These have been labeled "disordered," "wavy crystalline," and "crystalline," to

TABLE V. Relevant Voronoi polygon statistics for systems of 418 point particles. χ indicates the parameter defined in Eq. (4.1). Poisson and RSA rows indicate Voronoi polygon statistics for Poisson and random sequential addition configurations. The second and third columns represent the standard deviation of the number of edges and area of the Voronoi polygons. The mean number of edges $\langle E\rangle$ and area $\langle A\rangle$ for each of these systems are 6 and 2.392344×10^{-3}, respectively.

χ	$\frac{1}{N-1}\sqrt{\Sigma_{i=1}^{N}(E_i-\langle E\rangle)^2}$	$\frac{1}{N-1}\sqrt{\Sigma_{i=1}^{N}(A_i-\langle A\rangle)^2}$
0.033493		4.013836×10^{-4}
0.126794	5.834784×10^{-2}	1.215543×10^{-4}
0.222488	5.351538×10^{-2}	4.358028×10^{-5}
0.382775	3.668359×10^{-2}	1.915487×10^{-6}
0.495215	2.956553×10^{-2}	5.328853×10^{-7}
0.581340	1.918465×10^{-2}	5.859931×10^{-6}
0.779904	0	1.731724×10^{-8}
Poisson	6.541094×10^{-2}	6.181066×10^{-4}
RSA at saturation limit	3.806837×10^{-2}	5.310192×10^{-5}

be descriptive of the visual patterns presented by each. Starting with the unconstrained ideal gas configurations ($K=0$), they appear in that order as the cutoff radius K increases. In the disordered regime, only those collective coordinates $C(\boldsymbol{k})$ inside the $\boldsymbol{k}$-space cutoff radius K adhere to their minimum value $-N/2$. In the wavy crystalline regime, minimized $C(\boldsymbol{k})$'s occur not only inside the radius K, but also in finite patches beyond that radius, and as K increases those patches increase in size as well. These *exterior* minimizations are an implicit result of the nonlinearity of the transformation from particle coordinates to collective coordinates, (1.1) and (2.3). Finally, the crystalline regime presents infinite sets of minimized collective coordinates that percolate throughout $\boldsymbol{k}$ space, interrupted only by Bragg peaks in unstrained crystals, and local clusters of nonminimized collective coordinates surrounding Bragg peaks in strained crystals.

Evaluation of pair correlation functions and construction of Voronoi tessellations produce further characterization of particle configurations in each of these three regimes. Even within the disordered regime, an increase in K causes reorganization of the particle configurations in such a way as to produce an effective repelling core acting between neighboring particle pairs that is evident in the pair correlation function. Voronoi polygons change their character with increasing K from predominantly irregular and diverse in area and edge number, to substantially less diverse and more regular in the wavy crystalline regime, and finally to all identical polygons in the crystalline regime. In this evolution, the locations of the particles within their enclosing Voronoi polygons statistically drift toward polygon centroids, and become centers of inversion symmetry in the crystal regime.

Numerical data from the several system sizes investigated ($N=12$, 56, 168, and 418) indicate that in the infinite system limit, the disordered to wavy crystalline transition occurs when the number of independent constraints on collective coordinates reaches approximately 58% of the total number $2N$ of particle degrees of freedom present. The subsequent wavy crystalline to crystalline transition has been more difficult to locate in the large system limit owing to its slow drift with N (see Table IV). We can only conclude that in the infinite- N limit the wavy crystalline to crystalline transition requires that the number of minimized $C(\boldsymbol{k})$'s be some number between 80 and 100% of the total number of degrees of freedom. It should be noted that in one dimension, 50% is the corresponding infinite-system threshold for complete ordering (crystallization), and $33.3\cdots\%$ is the threshold for appearance of implicitly minimized collective coordinates [10].

TABLE VI. Investigation of similarities between configurations generated by our numerical search algorithm and the RSA process (at the saturation density) by three separate statistical measures. The second column indicates the approximate χ value for configurations similar to the saturated RSA system for each parameter used in the comparison.

Other statistical measures	χ
Standard deviation in Voronoi polygon edge number	0.370813
Standard deviation in Voronoi polygon area	0.196172
Radial distribution function	0.495215

Although our numerical studies have assumed a unit square as the system container, it is more generally the case that the size of this square could be varied. The spacing of wave vectors in $\boldsymbol{k}$ space is inversely proportional to the square's edge length. Consequently, holding the particle number N and cutoff radius K fixed, compression reduces the number of $C(\boldsymbol{k})$'s that are explicitly minimized. Therefore, compression applied to an initially crystalline system can cause it to undergo successive phase transitions to the wavy crystalline state, and then to the disordered state.

Thse most obvious extension of the present investigation is to examine the behavior of three-dimensional particle systems subject to an analogous set of collective coordinate minimizations. One might reasonably anticipate that once again a sequence of configurational transitions involving disordered, wavy crystalline, and crystalline states would be observed as the cutoff radius K increased from zero. But whether only three distinguishable regimes, or a larger number with more elaborate distinctions, would appear remains to be determined.

ACKNOWLEDGMENTS

The authors gratefully acknowledge D. K. Stillinger for carrying out a comprehensive set of preliminary calculations that has provided useful guidelines for the work reported in this paper. S.T. and F.H.S. gratefully acknowledge the support of the Office of Basic Energy Sciences, DOE, under Grant No. DE-FG02-04ER46108. O.U.U. gratefully acknowledges the support of the DOE CSGF program.

[1] D. Pines, Solid State Phys. **1**, 367 (1955).
[2] R. P. Feynmann, *Statistical Mechanics* (Benjamin, Reading, MA, 1972).
[3] M. J. Mandell, J. P. McTague, and A. Rahman, J. Chem. Phys. **64**, 3699 (1976).
[4] J. K. Percus and G. J. Yevick, Phys. Rev. **110**, 1 (1958).
[5] H. C. Andersen and D. Chandler, J. Chem. Phys. **53**, 547 (1970).
[6] E. Leutheusser, Phys. Rev. A **29**, 2765 (1983).
[7] P. G. Debenedetti, *Metastable Liquids: Concepts and Principles* (Princeton University Press, Princeton, NJ, 1996), pp. 282–301.
[8] M. Tanemura and M. Hasegawa, J. Theor. Biol. **82**, 477 (1980).
[9] C. W. Misner, K. S. Thorne, and J. A. Wheeler, *Gravitation* (W.H. Freeman, San Francisco, 1973).
[10] Y. Fan, J. K. Percus, D. K. Stillinger, and F. H. Stillinger, Phys. Rev. A **44**, 2394 (1991).
[11] S. Torquato and F. H. Stillinger, Phys. Rev. E **68**, 041113 (2003).
[12] *Handbook of Mathematical Functions*, edited by M. Abramowitz and I. A. Stegun, National Bureau of Standards Applied Mathematics Series No. 55 (U.S. Government Printing Office, Washington, D.C., 1970).
[13] N. W. Ashcroft and N. D. Mermin, *Solid State Physics* (Saunders College Publishing, Philadelphia, 1976), pp. 343.
[14] W. H. Press, B. P. Flannery, S. A. Teukolsky, and W. T. Vetterling, *Numerical Recipes* (Cambridge University Press, Cambridge, 1986).
[15] A. Okabe, B. Boots, and K. Sugihara, *Spatial Tessellations: Concepts and Applications of Voronoi Diagrams* (Wiley, New York, 1992).
[16] S. Torquato, *Random Heterogeneous Materials: Microstructure and Macroscopic Properties* (Springer-Verlag, New York, 2002).
[17] I. Hodder and C. Orton, *Spatial Analysis in Archaeology* (Cambridge University Press, Cambrige, 1976).
[18] E. Pielou, *Mathematical Ecology* (Wiley-Interscience, New York, 1977).